Cross-shelf thermal variability in southern Lake Michigan during the stratified periods

Cary D. Troy,[1] Sultan Ahmed,[1] Nathan Hawley,[2] and Allison Goodwell[3]

Received 22 March 2011; revised 23 November 2011; accepted 15 December 2011; published 18 February 2012.

[1] Results from a field experiment in southern Lake Michigan are used to quantify the cross-shelf nearshore variability in Great Lakes temperatures during the stratified season. The experiment was conducted along the Indiana coast of southern Lake Michigan, with temperature and velocity moorings arranged in a cross-shelf transect that extended to approximately 20 km from shore (40 m depth). The field site is noteworthy because of its location at the end of a major axis of an elliptical Great Lake, the relatively mild bathymetric slope, and local shoreline orientation that is perpendicular relative to the dominant summer winds. Measurements demonstrate that the location of the thermocline-bottom intersection is highly variable, causing a wide zone of extreme thermal variability in the nearshore region with time scales of variability ranging from hours to months. Near-inertial internal Poincaré waves are shown to cause large thermocline excursions but primarily only during periods of elevated activity. Several full upwelling events were observed, but in general, they were brief, lasting only 1–2 days, and had very limited spatial extent (2.5 km or less). Nonetheless, the offshore extent of the upwelling front was shown to be reasonably estimated with a simple estimate of the cross-shelf transport caused by alongshore wind events. A persistent feature that determined the zone of elevated thermal variability (the thermocline-shelf intersection point) was the strongly tilted thermocline, which resulted in the thermocline being located very close to shore. No evidence was found to support the hypothesis that internal Kelvin waves affect thermal variability at the study location.

Citation: Troy, C. D., S. Ahmed, N. Hawley, and A. Goodwell (2012), Cross-shelf thermal variability in southern Lake Michigan during the stratified periods, *J. Geophys. Res.*, *117*, C02028, doi:10.1029/2011JC007148.

1. Introduction

[2] The movements and dynamics of the summer thermocline in the coastal regions of the Laurentian Great Lakes have important consequences for cross-shelf and vertical exchange, thermal conditions experienced by biota, and nearshore water quality in the Great Lakes [*Rao and Murthy*, 2001b; *Rao and Schwab*, 2007]. These thermocline movements cause the nearshore region to be an environment of extreme thermal variability during the stratified period. *Wells and Parker* [2010] highlighted some of the biological consequences of this variability, which include setting the abundance and diversity of both native and invasive species [*Heufelder et al.*, 1982; *Haffner et al.*, 1984; *Wilson et al.*, 2006]; *Lee and Hawley* [1998] demonstrated the effects of thermocline movement on the transport of suspended sediment. The present work focuses on quantifying the cross-shelf distribution of nearshore thermal variability in southern Lake Michigan, and linking the observed variability with physical processes.

[3] Several physical mechanisms are known to cause nearshore thermocline excursions in large stratified lakes, and these mechanisms were initially hypothesized to be responsible for the nearshore thermal variability presented herein [*Rao and Schwab*, 2007]. The mechanisms considered in this work are wind-driven upwellings, internal Kelvin waves, and near-inertial internal Poincaré waves.

[4] Locally generated upwellings and downwellings typically occur as a result of locally applied alongshore or offshore winds, and can be accompanied by massive cross-shelf thermocline excursions and strong currents [*Csanady*, 1975, 1977; *Rao and Murthy*, 2001a, 2001b]. For large, rotation-affected lakes such as the Great Lakes, upwelling events typically occur on coasts to the left of the dominant summer winds, which is the western (Wisconsin) coast for the case of Lake Michigan (Figures 1 and 2). The spatial and temporal extent of these upwelling events can be quite large [*Mortimer*, 2004]; thermal satellite imagery taken during the time of the experiment described herein (summer 2009) shows persistent, widespread upwelling along much of the

[1]School of Civil Engineering, Purdue University, West Lafayette, Indiana, USA.
[2]Great Lakes Environmental Research Laboratory, NOAA, Ann Arbor, Michigan, USA.
[3]Ven Te Chow Hydrosystems Laboratory, University of Illinois at Urbana-Champaign, Urbana, Illinois, USA.

0148-0227/12/2011JC007148

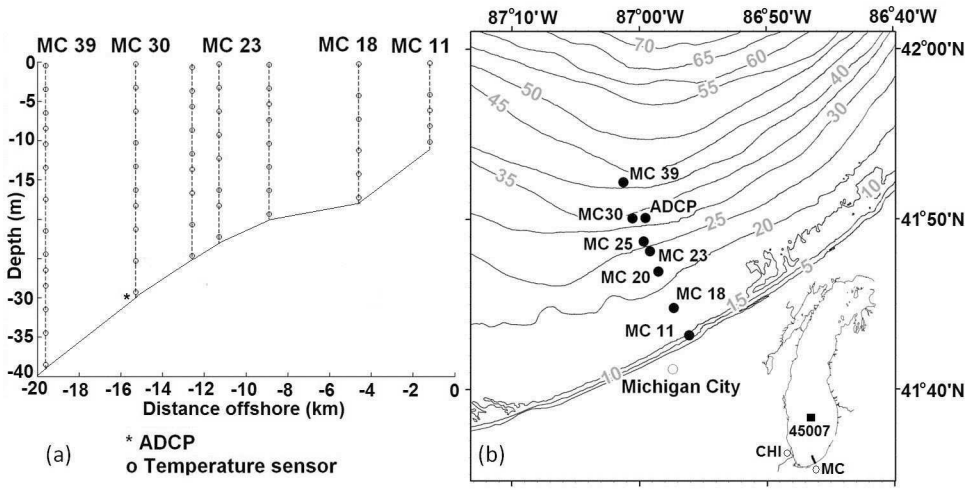

Figure 1. Field experiment location in southern Lake Michigan, near Michigan City, Indiana (United States). Seven thermistor chains were arranged in a cross-shelf transect, to depths of 40 m (20 km offshore; contours shown in m). An acoustic Doppler current profiler (ADCP) was located next to the 30 m mooring, and suspended sediment transmissometers recorded sediment concentrations near the bottom of the 20 and 30 m moorings. Also shown is the location of NOAA buoy 45007, which records standard meteorological, wave, and water properties, and both the Michigan City (MC) and Chicago (CHI) meteorological stations.

Wisconsin coast for much of August and September; this was also found for multiple years in the climatological numerical simulations of *Beletsky et al.* [2006], as well as Lake Michigan satellite imagery investigated by *Plattner et al.* [2006], and is in keeping with the generally southwesterly winds experienced by Lake Michigan during summer.

[5] Internal Kelvin waves are another cause for nearshore thermal variability in the Great Lakes, and their propagating fronts can induce local thermal changes on time scales ranging from hours to days [*Csanady*, 1972, 1975, 1977; *Csanady and Scott*, 1974; *Schwab*, 1977; *Beletsky et al.*, 1997; *Mortimer*, 2004]. Internal Kelvin waves can result from the relaxation of upwelling/downwelling zones, with

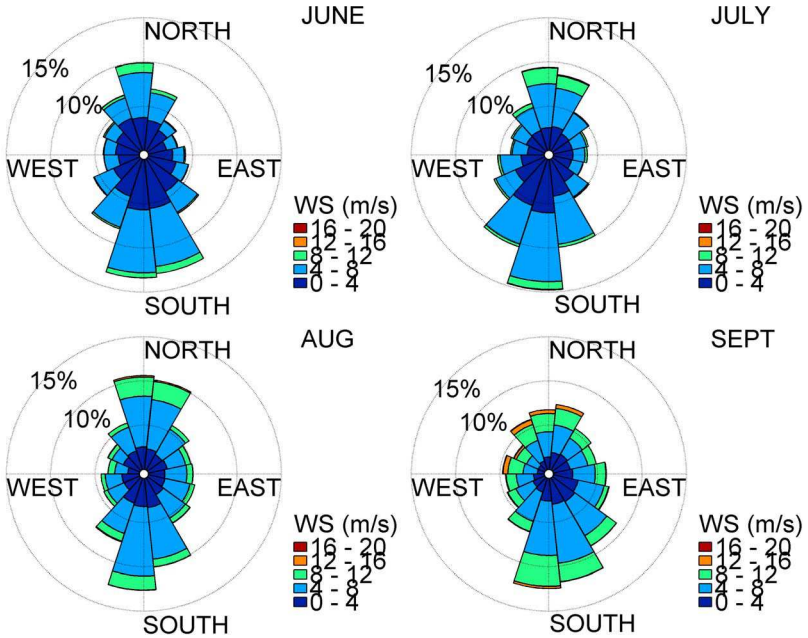

Figure 2. Wind roses for NOAA buoy 45007 in the southern basin of Lake Michigan for summer months averaged over the years 2000–2009. Direction indicated is that from which wind is blowing. Concentric rings (5, 10, and 15) give percentage of time wind is from that particular direction; colors within a wedge represent the relative proportion of time the winds from that direction are of a certain magnitude.

the upwelled/downwelled region propagating slowly in a cyclonic direction around large lake basins in the northern hemisphere [*Beletsky et al.*, 1997; *Antenucci and Imberger*, 2001]. These waves were identified in Lake Ontario by *Csanady* [1977], but to our knowledge, the only documented observed internal Kelvin wave events in Lake Michigan are the 1947 and 1955 events presented by *Mortimer* [2004] (the 1955 event was simulated by *Beletsky et al.* [1997]). While internal Kelvin waves can be identified by their spectral signature in smaller lakes [e.g., *Rueda et al.*, 2003; *Antenucci et al.*, 2000], the size of Lake Michigan renders the theoretical internal Kelvin wave period on the order of 1 month, over which meteorological variability will likely reset conditions, erasing any potential Kelvin wave spectral signatures [e.g., *Gómez-Giraldo et al.*, 2006].

[6] A third flow structure potentially responsible for nearshore thermocline motions is near-inertial Poincaré waves. Here "near inertial" refers to waves with periods slightly less than the local rotation period of the earth, which is approximately 17.5 h for southern Lake Michigan. In the Great Lakes, a broad spectrum of internal waves has been observed, but internal waves of near-inertial period are typically dominant, readily observed from temperature moorings and velocity data [e.g., *Csanady*, 1975; *Murthy and Dunbar*, 1981; *Mortimer*, 2004, 2006; *Hawley*, 2004]. Because of their near-inertial periods, Poincaré waves in Lake Michigan are perhaps more accurately classified as rotational waves that are weakly modified by thermal stratification, inducing large currents in the lake's interior with vanishing, but still persistent influence near the lake shores. Because most of the energy in these waves is kinetic, vertical thermocline displacements associated with these waves are modest, rarely more than several meters. It was therefore hypothesized that Poincaré waves would have limited influence on nearshore thermal structure; however, most analytical models of Poincaré waves [e.g., *Antenucci and Imberger*, 2001] are for flat-bottomed lakes and cannot capture the wave dynamics at the thermocline-shelf intersection.

[7] This paper describes a set of observations along Lake Michigan's southern shore that were designed to quantify cross-shelf thermal variability induced by thermocline motions during the stratified period. In particular, the work aims to quantify (1) the position of the summer thermocline along the lake shelf as a function of time, (2) the spatial and temporal characteristics of near-bottom thermal fluctuations induced by the moving thermocline, and (3) the physical processes causing this variability. This paper is organized as follows: Section 2 describes the experimental transect, including the field site location and instrumentation. Section 3 describes the physical processes and variability observed during the experiment, including temperatures, thermal transects, and currents. Section 4 presents quantifications of the thermal variability and links to physical processes, and section 5 presents a summary of the results.

2. Field Experiment Description

2.1. Field Site

[8] The field location selected was Lake Michigan's southern shore, near Michigan City, Indiana (Figure 1), which is a shore that receives pressure from both heavy industry (e.g., steel mills, refineries) and recreation (boating, beaches, and fishing). Lake Michigan, the second largest of the five Laurentian Great Lakes, is approximately 500 km long and 135 km wide, and is divided into two main basins by a submerged midlake plateau extending between Milwaukee, Wisconsin, and Muskegon, Michigan (Figure 1). Maximum depths exceed 250 m in the northern basin and exceed 150 m in the southern basin.

[9] The shore at the study site is characterized by a very mild bathymetric slope (40 m depth: 20 km distance, 0.002) and a sandy bottom (fine sand, $d \approx 0.1$ mm). As described later, this mild slope is one of the reasons that this location has such dramatic variability in the thermocline position along the lake shelf: vertical thermocline motions translate to large lateral excursions here. This variability occurs in spite of the dominant summer winds being north-south aligned and therefore not upwelling or downwelling favorable for most of the summer period.

[10] The location is also notable because of its location on the "minor shore" of one of the elongated, elliptically shaped Great Lakes (Lakes Ontario and Erie are the two others); more attention has been paid to the longer shores that are often treated as infinite coastlines, with the ends not typically treated in idealized analyses. For purposes of analysis later in the paper, the alongshore direction was taken as 70° clockwise from north.

[11] Lake Michigan's summertime southern basin circulation is quite variable and there is a need for additional measurements to validate current models there [*Beletsky and Schwab*, 2001, 2008]. *Beletsky et al.* [2006] and *Beletsky and Schwab* [2008] show with model results that while the flow in the southern basin of Lake Michigan is quite variable, the flow close to the lakeshore at the study location is generally anticyclonic (toward the west) during the summer period, with flow farther offshore being cyclonic.

2.2. Instrumentation

[12] An array of instrumentation was deployed in a 20 km long cross-shelf transect arrangement from 24 June 2009 to 9 October 2009 (Figure 1 and Table 1), which correspond to the Julian days of year 2009 (hereafter DOY) 175–282. The period of the study covered most of the stratified season for this location, beginning with weak, whole-water column stratification, and ending with the fall overturn for all but the deepest waters at the deepest (39 m) mooring. The transect arrangement is similar to earlier studies examining cross-shelf variability in the Great Lakes [*Murthy and Dunbar*, 1981; *Rao and Murthy*, 2001a], with more emphasis on cross-shelf, full water column thermal measurements.

[13] The instrumentation array included seven thermistor chains deployed along the cross-shelf transect at depths between 11 and 39 m (Table 1 and Figure 1), and an acoustic Doppler current profiler (ADCP) at 30 m depth. The spacing between thermistors on a given chain was designed to optimize spatial resolution near the expected thermocline position. The moorings were serviced twice during the deployment, on 24 July and 29 August. Several temperature sensors were used including RBR-TDRs, Seabird 39 s, and Onset U22 Pro v2s. Sample periods for the temperature sensors ranged from 2 s (RBR-TDR sensors) to 5 min (HOBO U22 pro V2). Mooring deployments, servicing, and recovery were carried out from the NOAA Great Lakes Environmental Research Laboratory (GLERL) R/V

Table 1. Locations and Details of Various Moorings and Instruments Deployed for 2009 Field Experiment in Southern Lake Michigan Near Michigan City, Indiana

Mooring	Depth (m)	Offshore Distance (km)	Thermistors	Other Instruments	Latitude, Longitude
MC11	11	1.2	5		41.7197°N, −86.9341°W
MC18	18	4.6	6		41.7491°N, −86.9456°W
MC20	20	8.9	8	transmissometer	41.7823°N, −86.9744°W
MC23	23	11.3	8		41.8023°N, −86.9853°W
MC25	25	12.6	9		41.8120°N, −86.9935°W
MC30	30	15.3	10	300 kHz ADCP transmissometer	41.8346°N, −87.0085°W
MC39	39	19.6	14		41.8707°N, −87.0198°W

Laurentian. The broadband ADCP was an RD Instruments 300 kHz unit mounted looking upward, 0.5 m above the bottom; 20 min ensembles were recorded every 20 min in 1 m bins between 3.7 and 26.7 m above bottom.

2.3. Meteorological Observations

[14] Standard meteorological data were acquired from the NOAA Michigan City and Chicago stations (MCYI3, 41.729°N, 86.913°W; CHII2, 41.912°N, 87.567°W) maintained by GLERL; the Michigan City wind sensor was only available after DOY 210. The Chicago wind data showed strong diurnal variability, presumably associated with sea breeze effects, that was only seen in the September Michigan City wind observations. The "alongshore" (roughly westward) estimated wind stresses at Chicago were persistently elevated relative to Michigan City, and this bias was removed for the upwelling calculations later in the paper. Additional weather data was obtained from NOAA buoy 45007 (42.674°N, 87.026°W) which is located in the center of the southern basin (Figure 1). This buoy also recorded surface water temperature, and wave height, period, and direction each hour. All wind speeds were adjusted to 10 m height using a wind speed–dependent drag coefficient, which was also used to estimate wind stress [*Wüest and Lorke*, 2003].

3. Observations

3.1. Meteorology

[15] Analysis of June–September wind data from NOAA Buoy 45007 for the years 2000–2009 showed that the dominant wind orientation for Lake Michigan's southern basin during this decade was along the north-south axis, with southerly winds dominating (Figure 2), and this was observed for much of the experiment (Figure 3). Monthly average wind speeds were within the normal range with the exception of September, which experienced relatively weak winds. Strong summer wind events were primarily from the south-southwest with a series of strong southerly wind events in late July and most of August (DOY 205–245). As seen in Figure 3, with winds mostly from the southwest, the majority of alongshore winds were downwelling favorable, whereas the offshore winds were upwelling favorable. While alongshore, upwelling-favorable events were rare, we show later in the paper that they were efficient at generating upwelling events when present.

3.2. Background Thermal Stratification

[16] The mooring array provided basic data illustrating the cross-shelf variability in thermal structure, including the seasonal evolution of thermal stratification (Figures 4 and 5). Animation S1 of the auxiliary material shows the interpolated cross-shelf thermal transect for the duration of the experiment.[1] The observed pattern of the formation and destruction of seasonal stratification generally mirrors what is already known about seasonal stratification in Lake Michigan [e.g., *Beletsky and Schwab*, 2001; *Mortimer*, 2004]. Early established stratification (1 July, DOY 182) was characterized by a diffuse thermocline extending over the entirety of the water column. A well-defined mixed layer and thermocline then formed, with the mixed layer deepening steadily through most of July (DOY182–212). For the remainder of the summer, the thermocline sharpened continuously in response to wind events, maintaining a relatively constant depth of 15–20 m. Following a large storm in early September (DOY 242), the stratification was weakened severely, and this weakening continued until several large storms in early October (>DOY 270) pushed the mixed layer to about 39 m depth, after which the water column was nearly isothermal at all moorings (Figure 4).

[17] As a metric of the strength of the thermal stratification at the different moorings, Figure 6 shows the daily averaged maximum Brunt-Väisälä frequency (N) found in the water column, for the 11, 20, and 39 m depth stations (here $N^2 \equiv (-g/\rho)(d\rho/dz)$, where ρ is the fluid density, g is gravity, and z is the vertical coordinate, positive upward). From Figure 6 it can be seen that as expected, the strength of the stratification increases and decreases with the summer heating and cooling, respectively, with maximum stratifications of N = 0.04–0.08 rad/s. The deepest (39 m depth) mooring appears "strongly stratified" at the end of the measurement period because of the lingering presence of the deepened thermocline, which had been pushed to nearly 39 m depth.

[18] The station closest to shore (MC11, 11 m depth) is seen to experience periodic, strong stratification, contrasting the notion that the nearshore waters are always well mixed; furthermore, the strength of this nearshore stratification can exceed the offshore stratification in rare occasions (e.g., DOY 230). Closer inspection of the raw temperature records (Figure 3) indicated that this changing nearshore stratification occurred because of fluctuating near-bottom temperatures and not surface heating and cooling, which has a small

[1] Auxiliary materials are available in the HTML. doi:10.1029/2011JC007148.

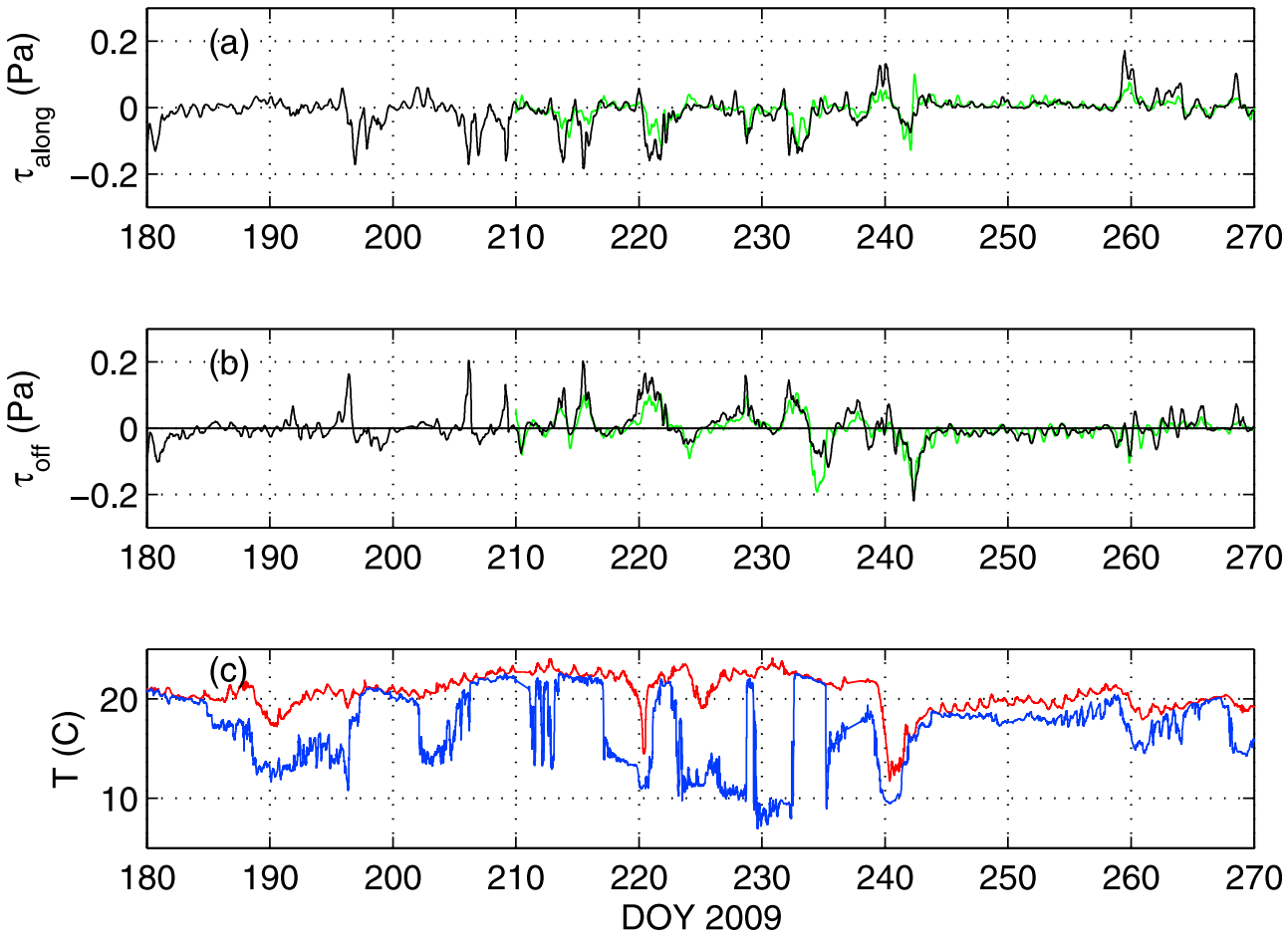

Figure 3. Wind stress and nearshore temperatures for the experiment. Shown are estimated (a) alongshore and (b) offshore wind stress estimated from Michigan City (green line) and Chicago (black line) meteorological stations. Wind data are smoothed with a 6 h moving window. The coastline orientation is taken as 70° clockwise from north, with positive alongshore stresses corresponding to winds from the north-northeast and positive offshore stresses corresponding to winds from the south-southeast. Upwelling-favorable winds are therefore positive in both Figures 3a and 3b. (c) The nearshore mooring (11 m depth) top and bottom temperatures, highlighting the relationship between nearshore thermal variability and local wind stress.

effect that is limited to the top several meters of the water column. Nearshore stratification during the experiment was generated primarily by thermocline excursions up the lake shelf into the nearshore region, and these excursions are discussed later in the paper.

[19] Also shown in Figure 6 is the depth of maximum thermal stratification in the water column, which is a dynamical indicator of the local effective thermocline depth. From this graph it is apparent that the thermocline was in a partially upwelled orientation for much of the experiment (this was also true of the isotherms themselves, as seen in the full 2-D transects, e.g., DOY 215–246, shown in Animation S1 and Figure 5), which is discussed further in section 3.3. This is in spite of the dominant basin wind patterns not being upwelling favorable (Figure 3), and therefore this feature was maintained not by local wind but rather by basin-scale circulation patterns (e.g., geostrophy associated with the alongshore pressure gradient caused by the quasi-steady southern basin cyclonic gyre).

3.3. Observations of Currents

[20] Full water column current data was provided by the single ADCP located at 30 m depth, 15 km offshore (Figure 7). On the basis of the strong near-inertial variability observed at this location and the classification scheme of *Murthy and Dunbar* [1981] and *Rao and Schwab* [2007], this ADCP mooring was located in the inertial boundary layer (IBL), where flow transitions from shore-parallel to open-lake motions. With respect to observed upwellings, the ADCP was offshore relative to the upwelled front and therefore indicative of flow in the outer shelf [*Austin and Lentz*, 2002].

[21] The ADCP data are shown in Figure 7, and several important features (described in more detail below) are worth noting. Strong baroclinicity is present in the velocity profiles, and much of this baroclinicity is associated with near-inertial (Poincaré wave) periodicity, which is present throughout the record. Additionally, strong westward velocities are seen in the surface layer for much of August

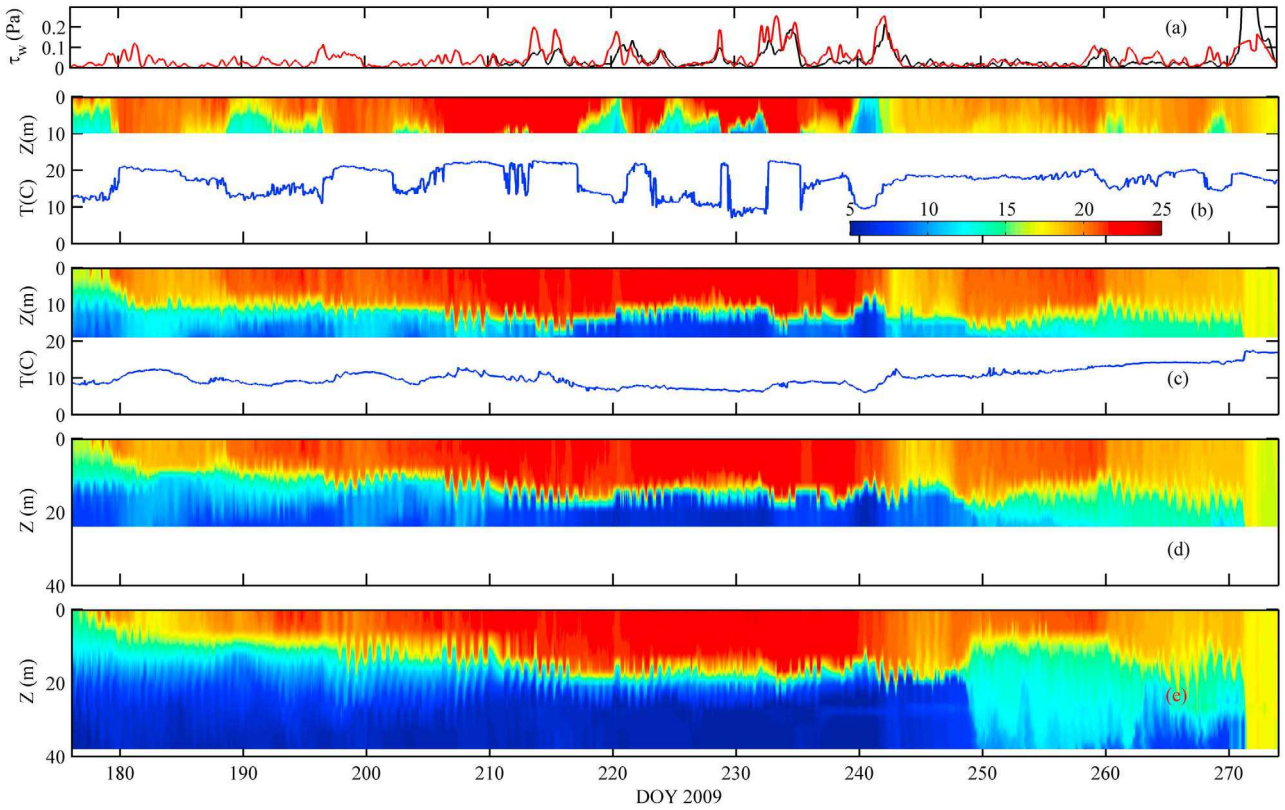

Figure 4. (a) Wind stress from buoy 45007 (red line) and Michigan City (black line) wind sensors. Whole–water column temperatures for (b) 11 m, (c) 20 m, (d) 25 m, and (e) 39 m depth moorings are also shown. Also shown are bottom temperature records for 11 m (Figure 4b) and 20 m (Figure 4c) moorings.

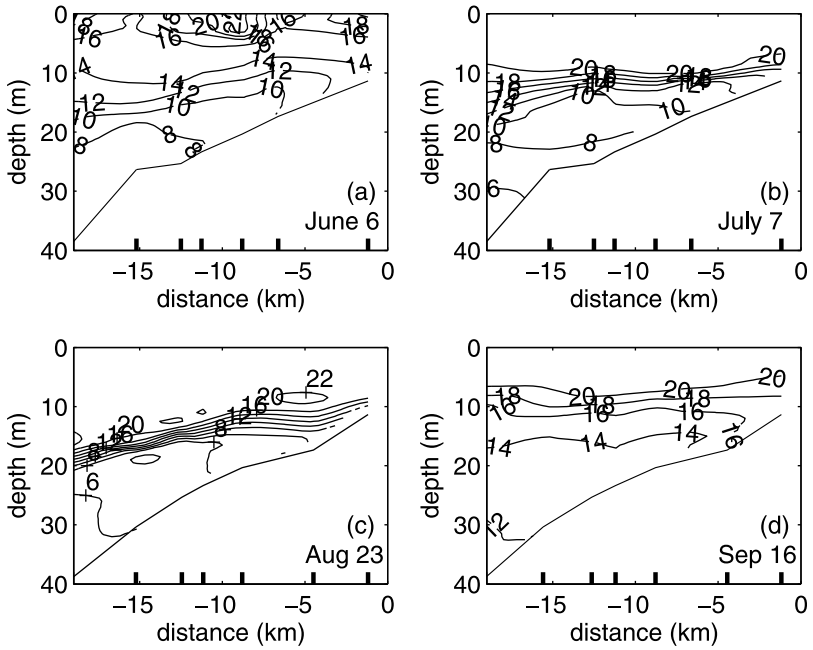

Figure 5. Cross-shelf variability of thermal stratification as observed with the mooring array. Shown are (a) the diffuse stratification, (b) well-formed thermocline, (c) sharpened thermocline, partially upwelled (which was consistently observed for most of August and September), and (d) diffuse thermal stratification. The seven mooring locations are shown as short vertical lines along the *x* axis.

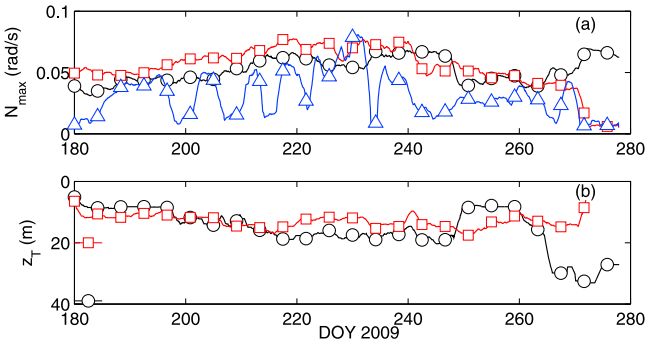

Figure 6. (a) Daily averaged maximum buoyancy frequency (N_{max}) found in the water column at the 11 m mooring (blue triangles), 20 m mooring (red squares), and 39 m mooring (black circles). (b) Observed thermocline depth, defined as the location of N_{max}, for 20 and 39 m moorings, with symbols as in Figure 6a. Note day of year (DOY) 210–245, during which the thermocline was persistently partially upwelled.

(DOY 215–245), which were part of a prolonged coastal jet structure. Finally, barotropic periodicity with a time scale of several days is seen near DOY 235–245, which appears to have been the signature of the Lake Michigan southern basin vortex mode [*Saylor et al.*, 1980].

[22] The observed flow can be broken into the three general periods shown in Figure 8, where progressive vector diagrams are shown for flow above and below the thermocline. First, for DOY 180–210, flow was weak and in the offshore (toward northwest) direction – both above and below the thermocline. This was followed by a period of strong alongshore westward flow (DOY 210–240), which was associated with the upwelled thermocline described earlier; this westward flow was very strong in the surface layer, and weaker in the bottom layer. The final period (DOY 240–270) was characterized by relatively strong eastward, alongshore flow both above and below the thermocline. The current reversal that began this eastward flow occurred first below the thermocline several days prior to the reversal in the upper layer. The currents after DOY 270, when the water column was isothermal, were alongshore,

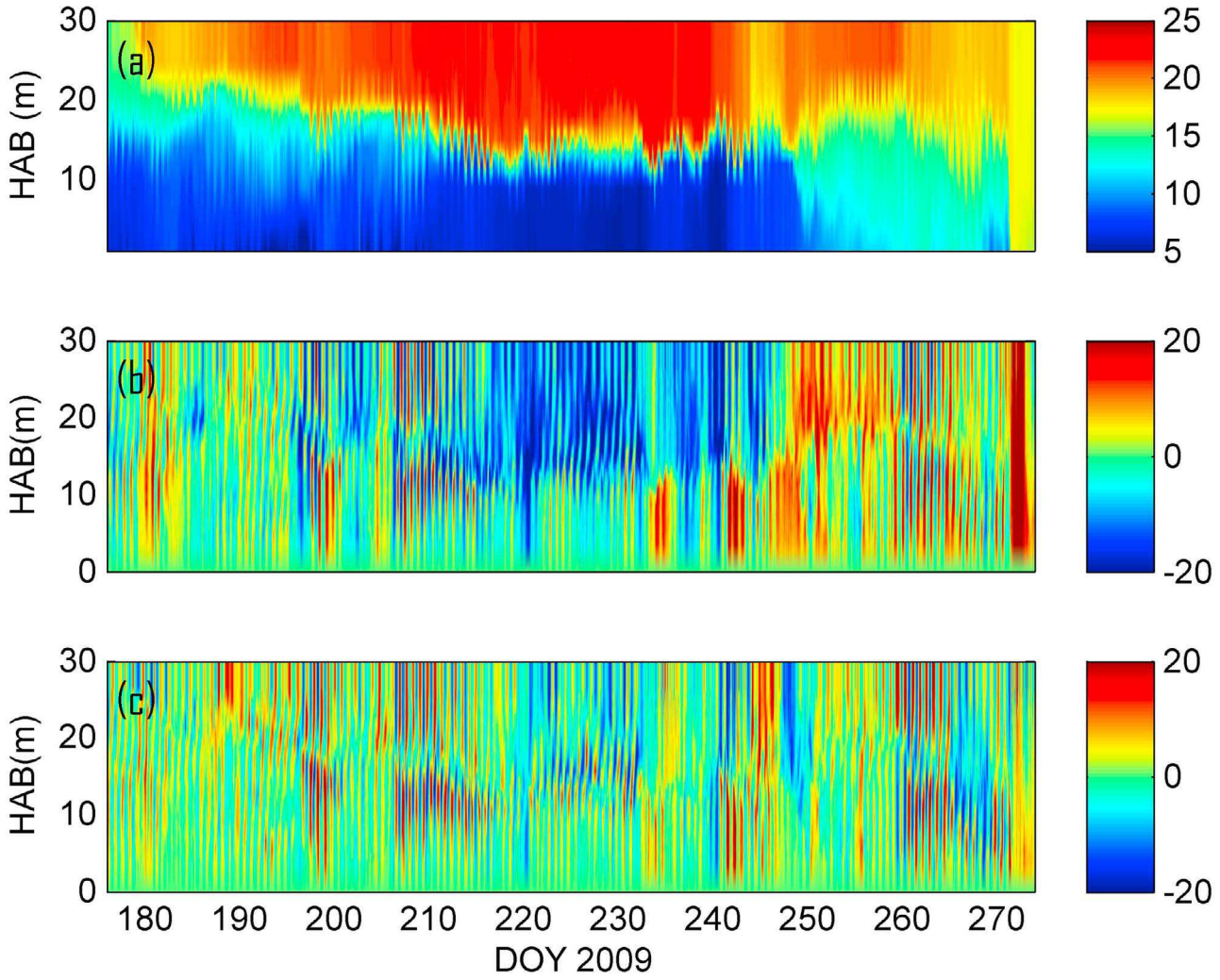

Figure 7. Temperatures and velocities from the 30 m station. Shown are (a) water temperatures (°C), (b) eastward velocities (cm/s), and (c) northward velocities (cm/s).

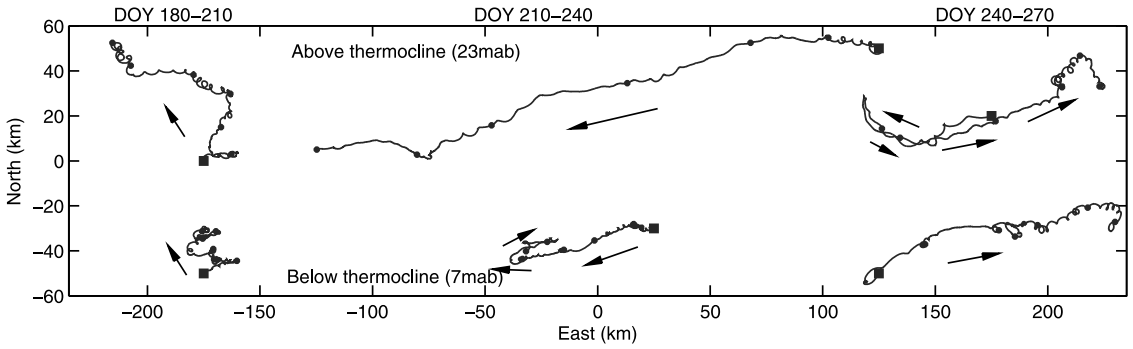

Figure 8. Pathline diagram (hodograph) based on velocities above (top diagrams, 23 m above bottom (mab)) and below (bottom diagrams, 7 mab) the thermocline for three primary periods during the experiment. Pathlines start with solid squares, and positions at 5 day increments are marked with solid circles. The coordinate origin is arbitrary, but travel distance magnitudes have been preserved.

primarily eastward (cyclonic) and strong, and in the same direction over the entire water column (Figure 7).

[23] To better characterize the physical processes observed throughout the experiment, wavelet analysis was carried out on the velocity data using the procedures described by *Liu and Miller* [1996]. Both linear and rotary wavelet analysis were performed separately on raw ADCP velocity bin signals, with clockwise spectra showing the most discernable features in the data. Analysis was also performed on depth-integrated velocities in order to isolate barotropic processes. The wavelet calculations were performed using the Morlet wavelet, with a Matlab code provided by C. Torrence and G. P. Compo (http://atoc.colorado.edu/research/wavelets), and wavelet parameter set to 5.336 [*Rao and Murthy*, 2001c]. All vertical bins showed similar temporal and frequency structure, with more energy for near-surface velocities.

[24] Figure 9 shows the raw velocities and clockwise rotary wavelet spectra for a vertical location 5 m above bottom, which qualitatively mirrors what can be seen at other depths. Two key features are evident. First, near-inertial energy is clearly present for most of the experiment (even more so at other depths), manifested as the thin band of clockwise energy at the inertial frequency (conventional spectra verified that this band was indeed almost entirely because of near-inertial energy). This is in keeping with the near-inertial, clockwise-rotating velocities associated with low-mode internal Poincaré waves in large lakes [*Antenucci and Imberger*, 2001; *Mortimer*, 2004].

[25] To highlight the temporal structure of the near-inertial energy, the maximum energy at near-inertial periods is also shown in Figure 9c, from which the episodic nature of these Poincaré wave events can be seen, including the large event that occurred from DOY 205 to 220. Four clearly discernable Poincaré wave events are seen, DOY 197, 205–220, 240–245, and 260–265, and they generally follow large wind events (Figure 3); the duration of these events is roughly 3–5 days, with the exception of events that saw continued wind forcing. Corresponding near-inertial periodicity is seen in the nearshore temperature record (Figure 3), suggesting that the near-inertial influence on thermocline motions persists nearly to the lake shore, and highlighting internal Poincaré waves as a definite, if occasional, source of thermal variability in the nearshore region.

[26] The near-inertial energy is attributable to baroclinic wave motions as it is absent in an identical wavelet analysis performed on the depth-averaged (barotropic) flow; the temporal structure of the wavelet-derived near-inertial clockwise energy is also nearly identical to the temporal structure associated with energy in the first baroclinic mode, as determined by an empirical orthogonal function analysis (not presented).

[27] A large energy spike is seen in the clockwise wavelet spectra for all depths at 100 h period at DOY 235–245; this signal is even more pronounced in the depth-averaged wavelet spectrum, and similar periodicity is seen in the thermocline displacements during this time (Figure 7). The combined clockwise sense of rotation, strong barotropic character, and approximately 100 h time scale of this event point toward excitation of the vortex mode (topographic wave) described by *Saylor et al.* [1980] for Lake Michigan's southern basin, which appears to have been strongly excited by the near-perfect wind stress for this event, persisting for over a week. The clockwise rotary wavelet spectrum for the wind stress also shows an identical feature at this time, which saw strong westward (upwelling-favorable) winds followed by an equally strong eastward pulse (Figure 3). The sense of this wind event is consistent with the large upwelling and downwelling seen in the temperature records (Figure 3), with the alongshore velocities mirroring the wind stress. Therefore it seems that the large upwelling and subsequent downwelling seen at DOY 240 (Animation S1) is caused by local winds, but with the response heavily modified by the presence of the topographic vortex mode.

[28] Also evident from the ADCP record is the strong baroclinicity in the raw velocity profiles, in the form of a distinct vertically two-layered structure (vertical mode 1); this structure is most evident for the near-inertial oscillations, but is also present at times when subinertial flow dominates (DOY 210–245). Shown in Figure 10 is the empirical orthogonal function (EOF) decomposition of the vertical structure of the currents measured by the ADCP. For this analysis, the experiment was divided into periods of roughly similar stratification since the local stratification will determine the baroclinic modal structure. Figure 10 shows the modal amplitudes as a function of time for the first three modes: barotropic (no zero crossings), first baroclinic (one zero crossing), and second baroclinic (two zero crossings).

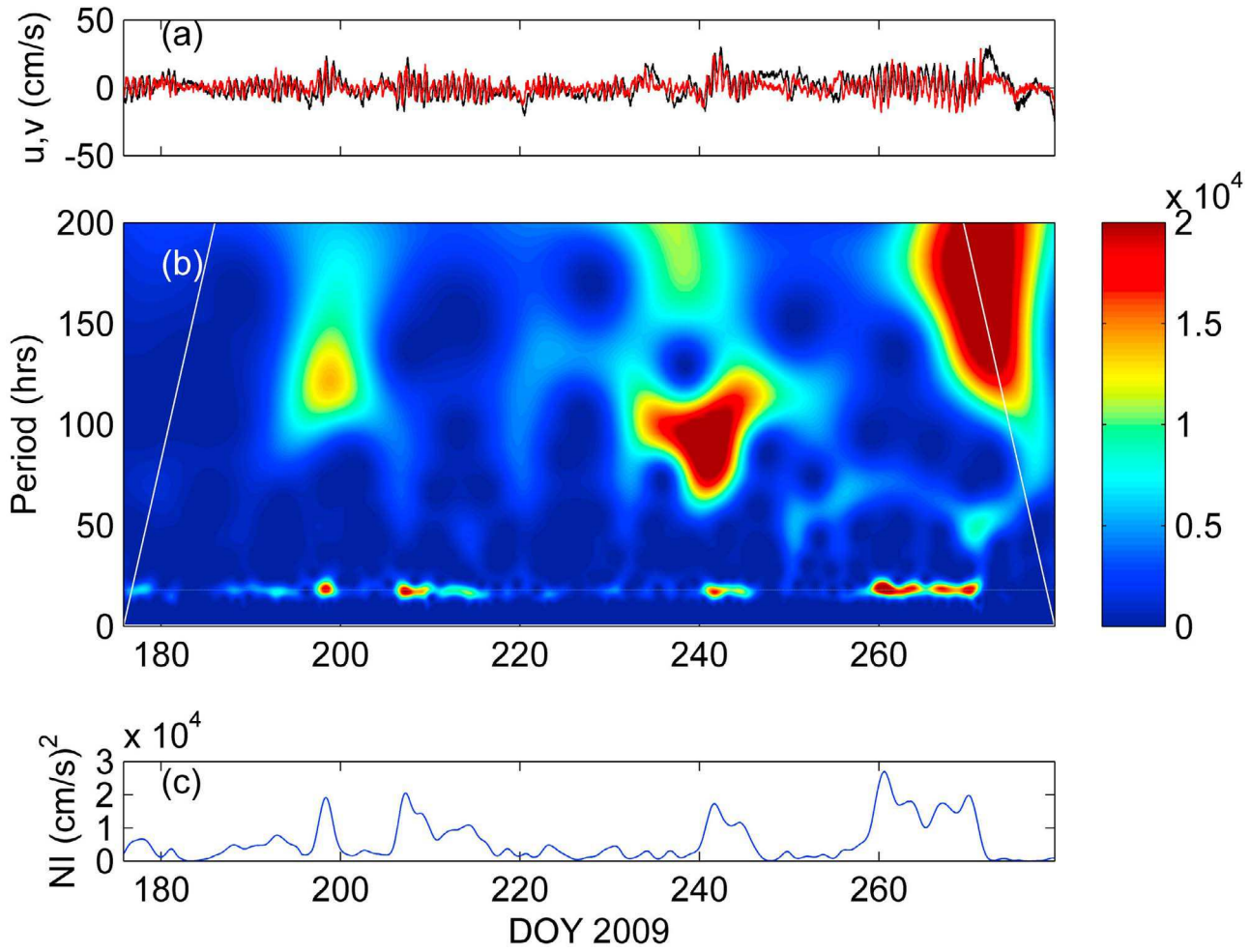

Figure 9. (a) Clockwise rotary wavelet spectrum for the east (black line) and north (red line) velocity signals at elevation 5 mab. (b) The near-inertial clockwise energy magnitude (with inertial period indicated as a dashed line), which shows discernable internal Poincaré wave energy persistence at the near-inertial period for the duration of the experiment, and (c) the clockwise wavelet spectrum ($(cm/s)^2$). Also seen is clockwise energy at 100 h time scales (DOY 240), which is consistent with Lake Michigan's southern basin topographic wave. The solid white lines in Figure 9b delineate the cone of influence of the wavelet calculation.

While EOF-derived modes are in no way constrained to be actual dynamical modes [*Edwards and Seim*, 2008], the found first and second baroclinic modes are here so termed because they were determined to be very similar to the calculated first and second baroclinic mode shapes for the normal modes solution for the observed thermal stratification [e.g., *Gill*, 1982].

[29] The temporal variation seen in the first baroclinic mode closely mirrors the temporal variation in the near-inertial energy shown in Figure 9, and closer inspection of the EOF results indicates that the observed superinertial baroclinic mode one signal is almost entirely at near-inertial period. Large mode 1 amplitudes are seen for the largest Poincaré wave events observed during the experiment (DOY 197, 205–220, 240–245, and 260–265). Some mode 2 energy is appreciable at times during the experiment, but it could not be determined whether this was indicative of actual higher-mode internal wave activity (isotherm spectra did not highlight any other frequencies other than diurnal and near inertial).

[30] The barotropic mode is dominant in the alongshore current profiles during the period of prolonged upwelling (DOY 220–250), during which the flow structure resembled a coastal jet, with strong alongshore flow both above and below the thermocline. It is additionally dominant during the presence of the vortex mode (DOY 235–245) illustrated in the wavelet spectra presented in Figure 9, as expected.

4. Cross-Shelf Thermal Variability

4.1. Near-Bottom Temperatures

[31] The impact of thermocline motions on mooring bottom temperatures is shown in Figure 11, which shows the near-bottom temperatures of 6 moorings throughout the experiment. At the mooring closest to shore (MC11, 11 m depth, 1.2 km offshore), near-bottom temperature fluctuations of more than 10°C are not uncommon, often occurring

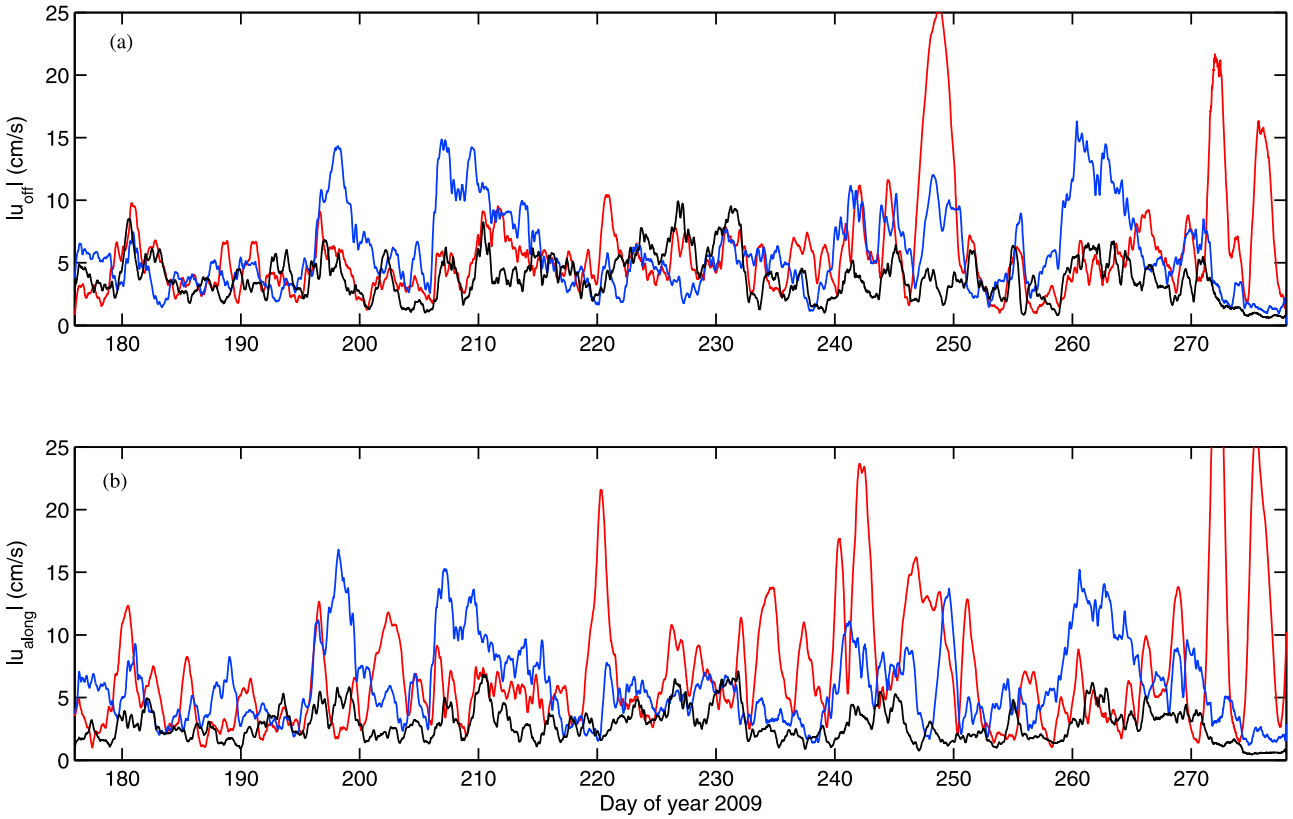

Figure 10. Velocity modal amplitudes derived from the empirical orthogonal function decomposition of the raw ADCP-derived velocity profiles. Shown are the barotropic (red lines), baroclinic mode 1 (blue lines), and baroclinic mode 2 (black lines) for the (a) offshore and (b) alongshore directions. The EOF modal amplitudes are smoothed to eliminate superinertial variability.

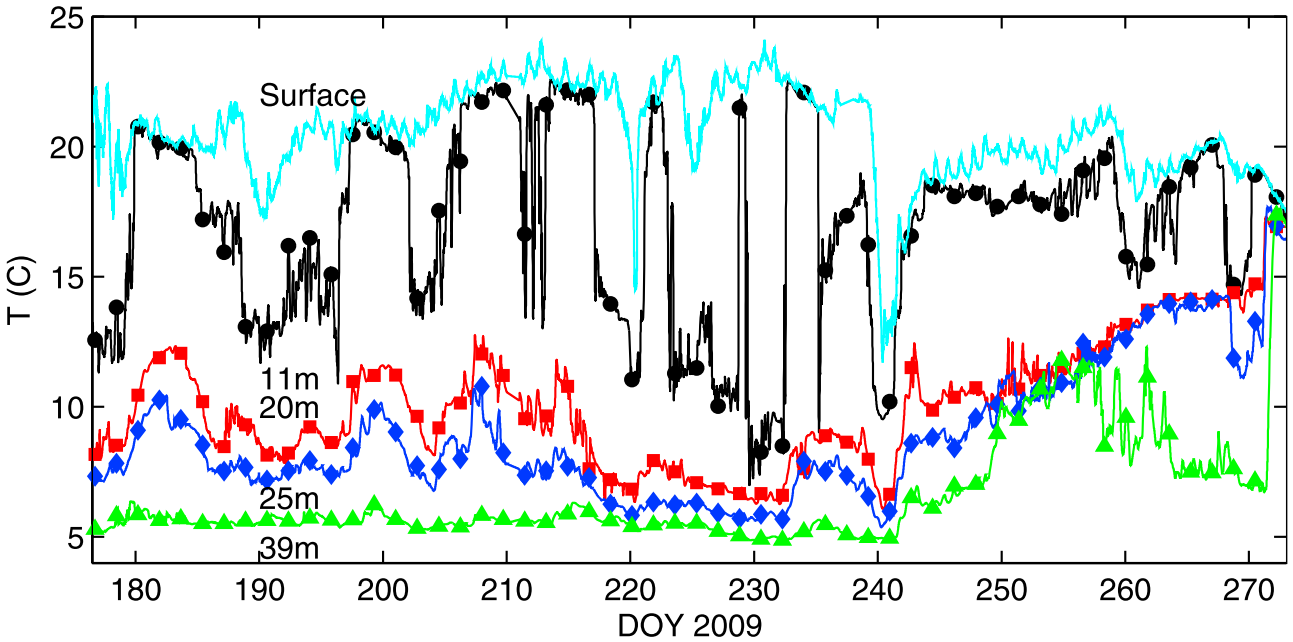

Figure 11. Near-bottom temperatures for 39, 25, 20, and 11 m depth moorings. Also shown is the surface temperature of the nearshore (11 m) mooring (top line). Full upwellings are shown as dramatic dips in surface temperatures (e.g., DOY 238), but the extreme variability in the nearest-shore bottom temperature suggests frequent movement of the lake thermocline along the shelf past this location.

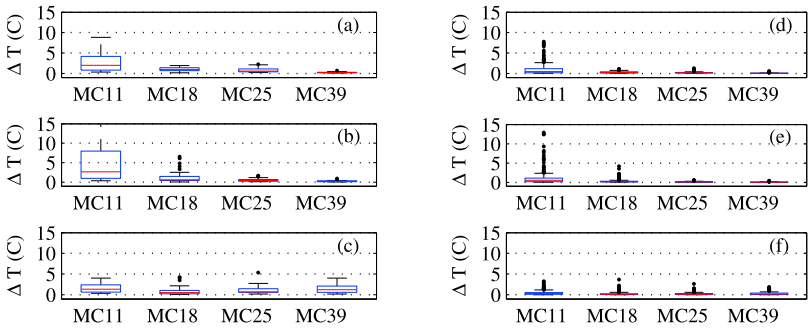

Figure 12. Distributions of thermal fluctuations calculated for (a–c) 24 h periods and (d–f) 3 h periods for four of the experimental moorings. Figures 12a and 12d are for July; Figures 12b and 12e are for August; Figures 12c and 12f are for September. The central red line indicates the median temperature fluctuation over the time scale (3 or 24 h); the boxes span the 25th and 75th percentiles, and the whiskers represent the bounds of data not believed to be outliers. Additional points are plotted as single dots.

on time scales of several hours or less. In contrast, full upwellings, are only seen rarely and briefly, suggesting that surface temperature measurements alone, such as those derived from satellite imagery, provide a subdued perspective of the true nearshore thermal variability, at least at this location in Lake Michigan.

[32] Rapid thermal variations, on various time scales, can cause lethal and sublethal effects in many aquatic organisms; the effects of these temperature changes on biota are dependent on the magnitude of these changes and the rate at which they occur [*Donaldson et al.*, 2008]. To quantify the spatial variability of the near-bottom thermal variations (not raw temperatures) experienced at different moorings, the maximum and minimum temperatures experienced over 3 h and 24 h moving windows were quantified; the difference between these maxima and minima yielded the temperature range experienced during that time window, a continuous metric of thermal variability at these 3 and 24 h time scales for each mooring. Figure 12 shows box and whisker plots for the distributions of near-bottom temperature ranges experienced over 3 and 24 h time scales for three study months (July, August, and September). During strong stratification (July and August), thermal variability decreases monotonically with distance offshore, whereas during weak stratification (September), thermal variability is smaller, and also more uniform across the lake shelf. The peak variability during the strongly stratified months of July and August occurred at the 11 m mooring because of its close proximity to the thermocline-shelf intersection. Thermal fluctuations in excess of 10°C, over 3 h are sometimes seen at the nearshore mooring, with median thermal fluctuations closer to 1–2°C, over a 3 h time scale.

4.2. Thermocline Position Along the Lake Shelf

[33] One of the primary goals of the experiment was to quantify the location and variability of the thermocline-shelf intersection. On the basis of the observed stratification, the thermocline was defined as being bounded by the 12°C and 18°C isotherms during the strongly stratified period. Measured bottom temperatures (Figure 11) were interpolated along the measurement transect, and the cross-shelf positions of the 12°C and 18°C isotherms were determined continuously as a function of time. The resulting location of the thermocline-shelf intersection is shown in Figure 13.

[34] In general, at this location, the thermocline covers a region that is typically located approximately 3–7 km offshore, from July through September; but this position is highly variable. The thermocline-shelf intersection is not a single location, but rather a zone several kilometers wide because of the mild slope at the study site. In general one would expect the shelf zone covered by the thermocline to scale as $\Delta y \sim \Delta z/S_0$, where S_0 is the cross-shelf bed slope and Δz is the thermocline thickness. With $S_0 = 0.002$ and with an observed $\Delta z \approx 7$ m, this yields a zone of variability of $\Delta y = 3.5$ km, which is reasonably close to the observations. In contrast, a more steeply sloped location like the eastern shore of Lake Michigan (Michigan, United States; Figure 1) would have a smaller zone of elevated thermal

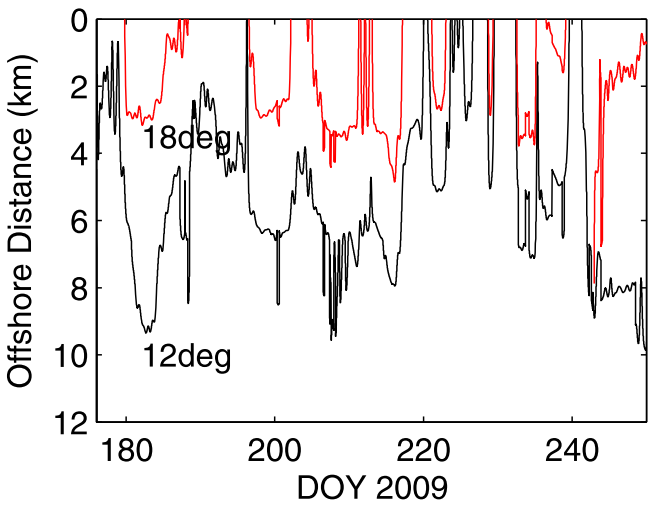

Figure 13. Thermocline-shelf intersection location, as defined by the interpolated location of the 12°C and 18°C isotherms. Calculation is not shown after DOY 250 because after that point, stratification is very diffuse and the thermocline is no longer well defined. Subinertial processes are responsible for the largest thermocline excursions, but near-inertial motions, when intense, e.g., DOY 205–210, do contribute to shorter-term variability in the thermocline position. Note that full-upwelling events register as zero displacement.

Table 2. Upwelling Event Displacements and Associated Event Parameters[a]

Event	Days	Ekman Layer Thickness δ_E (m)	Surface Layer Thickness (m)	Alongshore Wind Impulse I/ρ_0 (m^2/s)	Observed Offshore Displacement ΔX (km)	Theoretical Offshore Displacement $I/f\rho_0\delta_E$ (km)
1	189.5–191.2	11	**10**	1.9[b]	1.0	1.9
2	193.3–196.3	**9**	11	0.9[b]	0.3	1.3
3	216.7–220.4	**12**	17	2.8	2.0	2.4
4	223.6–226.5	**14**	17	2.9	1.5	2.1
5	231.4–232.0	**16**	16	0.7	0.5	0.5
6	238.7–240.9	21	**15**	4.8	4.5	3.2

[a]Variables are defined in text; bold thickness values indicate the smaller of the Ekman and surface layer thicknesses, which was the thickness used in estimated offshore frontal displacement.
[b]Chicago-derived alongshore wind stress, which was corrected to eliminate persistent (positive) bias relative to Michigan City observations.

variability closer to 1 km because of its steep slope ($S_0 \approx 0.006$).

[35] However, regions with steeper bathymetry also have colder water closer to shore, and may actually experience even greater temperature changes even with more moderate lateral thermocline excursions (preliminary analysis of a Muskegon, MI Lake Michigan experiment carried out in 2010 suggests this).

[36] From Figure 13 it can be seen that near-inertial motions play only a small role in the movement of the summer thermocline along the lake shelf, but episodes of intense Poincaré wave-induced variability do exist. Upon closer inspection, near-inertial periodicity is seen during the largest Poincaré episode (DOY 205–220), showing that the horizontal Poincaré wave-induced thermocline excursions can be large (that these high-frequency excursions are of near-inertial frequency is confirmed by the spectra of the raw temperatures, from which Figure 13 is derived).

[37] In general, the Poincaré wave-induced vertical thermocline motions are small, at most 3–4 m in total vertical displacement (Figures 4 and 7), even during the most energetic episodes, and the associated cross-shelf thermocline excursions are correspondingly at most $\Delta y \sim \Delta z/S_0 \sim 3$–4 m/0.002 = 1.5–2 km. That these waves still occasionally induce fairly substantial cross-shelf thermocline migrations at this location is thought to be primarily a function of the locally mild bathymetric slope, although this hypothesis should be tested at additional locations.

[38] This result – that internal Poincaré waves move the thermocline up and down the lake shelf by appreciable distances – is important because it provides an important link between traditional analytical models of Poincaré waves in flat-bottomed basins (for which no wave "run-up" can occur in spite of large thermocline oscillations at the lake boundary) and the behavior of the actual wave-induced motions along a real sloping boundary.

4.3. Local Wind Effects on Upwellings and Downwellings

[39] In Lake Michigan, with the dominant summer winds from the south-southwest, the western (Wisconsin) coast of the lake often sees persistent, widespread upwelling [*Plattner et al.*, 2006], and satellite imagery confirmed that this was the case for much of the field experiment. The southern Lake Michigan coast, where the field experiment was conducted, is not generally considered upwelling/downwelling favorable.

[40] Nevertheless, several full upwelling events were observed during the observation period, where surface temperatures at the mooring nearest shore dropped dramatically (Figures 11 and 13 and Animation S1). The duration of all of these surface upwelling events was brief, generally lasting only 3 days or less, and the offshore displacement was generally no more than 2.5 km. None of the upwellings were perceivable in the sea surface temperature (SST) imagery for the period and thus were highly localized. Additionally, most of the upwellings were associated with strong westward layer-averaged velocities in both the surface and bottom layers at the 30 m depth ADCP mooring.

[41] In rotational systems, prolonged alongshore winds can cause upwellings and downwellings [e.g., *Austin and Lentz*, 2002]. Very strong cross-shelf winds can also cause upwellings, as well as cause substantial cross-shelf exchange [*Csanady*, 1977]. However, the effect of cross-shelf winds is primarily felt in the surface mixed layer [*Tilburg*, 2003]. While offshore wind impulses were observed throughout the experiment (Figure 3), an application of the simplified offshore wind impulse analysis of *Csanady* [1977], which considers the necessary offshore wind impulse to cause upwelling in a flat-bottomed, two-layered system, indicated that these impulses were still far weaker than those required to cause thermocline upwelling.

[42] To examine the extent to which local alongshore winds, although rare, were responsible for the observed thermocline upwellings, a simple frontal displacement scaling provided by *Austin and Lentz* [2002] and *Tilburg* [2003] was tested. For the alongshore, upwelling favorable wind events, the offshore position of the upwelling front resulting from surface layer Ekman transport should scale as

$$\Delta X = \frac{I_{along}}{\rho_0 f \delta_E}, \tag{1}$$

where $I_{along} = \int \tau_{along}(t)dt$ is the total alongshore wind stress impulse for the event, τ_{along} is the alongshore wind stress, ρ_0 is the surface mixed layer density, f is the Coriolis parameter (10^{-4} s^{-1}), and δ_E is the smaller of the surface layer thickness and the theoretical Ekman layer thickness (see Table 2). The estimate (1) does not take into account the initial thermocline-shelf position or thermal stratification strength, and is expected to be valid for longer events having undergone full geostrophic adjustment. Nevertheless, it provides a bulk metric of the Ekman transport provided by alongshore, upwelling-favorable winds.

[43] For the calculation, a suitable midthermocline isotherm was used to infer the upwelled location from the thermal transects; upwelled locations closer to shore than the first mooring (1.2 km offshore) were estimated with

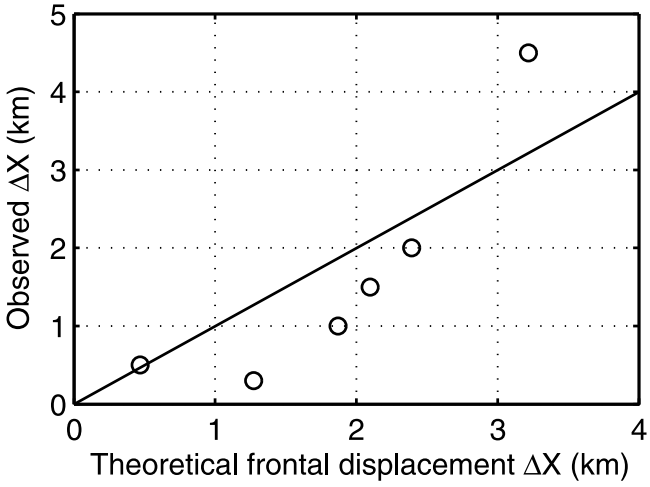

Figure 14. Observed and theoretical upwelling front offshore position for upwelling periods observed during the strongly stratified period (Table 2). The theoretical frontal displacement is calculated as the time-integrated offshore Ekman displacement associated with a steady alongshore wind, after *Austin and Lentz* [2002].

extrapolation. Wind impulses were determined by numerically integrating the alongshore wind stresses; some subjectivity exists in defining the wind impulse, but generally a well-defined alongshore impulse could be found prior to the observed upwellings.

[44] Figure 14 shows that the Ekman transport estimate agrees reasonably well with the observed upwelling front location, with larger alongshore wind impulses leading to large upwellings. Small displacements were overestimated by the formula; in addition to violation of the formula assumptions listed above, one possible explanation for the overestimation is the relatively strong stratification (the bulk water column stratification was roughly $N^2 = 1 \times 10^{-3}$ s^{-2} for most of the upwellings, i.e., $N/f \sim O(10^2)$), which should diminish the cross-shelf Ekman transport [*Tilburg*, 2003]. As *Tilburg* [2003] detail, this effect can be parameterized for idealized linear stratifications but for the discussion here the important point is that alongshore wind events, although rare, do seem to be responsible for the full upwellings observed during the experiment, and that a simple parameterization of the cross-shelf transport performs reasonably well in predicting the front location.

4.4. Persistent Cross-Shelf Thermocline Tilt

[45] For much of the experiment, a persistent cross-shelf thermocline tilt was observed, in a partially upwelled position (Figure 5 and Animation S1). This feature persisted for nearly 40 days (DOY 210–250), and placed the thermocline within close proximity to the shore, leading to large temperature fluctuations at the mooring nearest the shore (Figures 3 and 6). In addition to setting the location of elevated subsurface thermal variability, this feature is important in the context of explaining the observed thermal variability because it placed the thermocline close to shore, which allowed even the relatively weak alongshore wind pulses that occurred to cause full upwellings.

[46] Some insight into this persistent upwelling is provided from the low-passed velocity data from the 30 m ADCP. Figure 15 shows the vertically averaged velocities above and below the thermocline during this period, as defined by the regions above and below the 15°C isotherm position; near-inertial and superinertial motions are filtered out. As can be seen, this period was associated with very strong anticyclonic flow in the surface layer (toward the SW, alongshore direction) and weaker, but still generally anticyclonic flow in the bottom layer. This is also seen in the current trajectories shown in Figure 8.

[47] To better analyze the dynamics of this feature, the depth-integrated momentum balance was calculated from the ADCP data. Neglecting lateral friction, the linearized momentum balances for the vertically integrated alongshore (x) and offshore (y) velocities ($\bar{u}$ and $\bar{v}$, respectively) over a water column with depth H and Boussinesq density ρ are

$$\frac{\partial \bar{u}}{\partial t} - f\bar{v} = -g\frac{\partial \eta}{\partial x} + \frac{\tau_x^s}{\rho H} - \frac{\tau_x^b}{\rho H} \tag{2}$$

$$\frac{\partial \bar{v}}{\partial t} - f\bar{u} = -g\frac{\partial \eta}{\partial y} + \frac{\tau_y^s}{\rho H} - \frac{\tau_y^b}{\rho H} \tag{3}$$

Here $\eta(x, t)$ is the free surface displacement; τ_i^s is the surface wind stress in the i direction; and τ_i^b is the bottom stress opposing motion in direction i. The acceleration and Coriolis terms were calculated directly from the depth-integrated velocities (Figure 15). The wind stresses were estimated from the meteorological data as described earlier, and the bottom stress for direction i was parameterized with a drag coefficient as $\tau_i^b = C_d\rho|u_i^b|u_i^b$, where u_i^b was the near-bottom velocity in the i direction [*Trowbridge and Lentz*, 1998]. The bottom drag coefficient was taken as $C_d = 0.002$ [*Saylor and Miller*, 1988], but in general at this (relatively deep) location

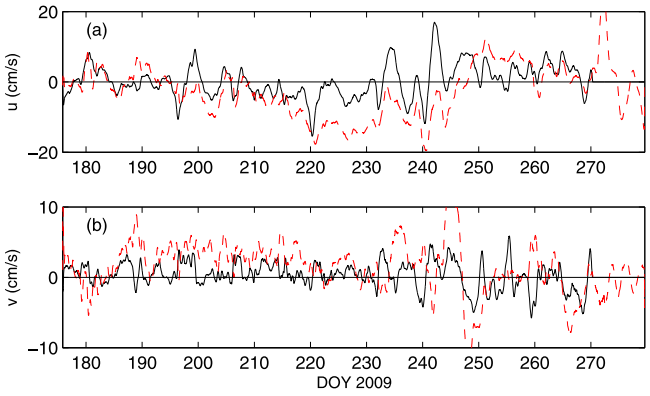

Figure 15. (a) Alongshore and (b) offshore layer-averaged velocities in surface (dashed lines) and bottom (solid lines) layers. Data are averaged at an 18 h period to remove inertial oscillations. Surface and bottom layers are defined as the regions above and below the daily 15°C isotherm position, and the positive alongshore direction is defined as 70° clockwise from north, e.g., flow toward the west-southwest during days 210–245. Note the offshore velocity scale is one half the alongshore scale and is defined as positive in the offshore direction.

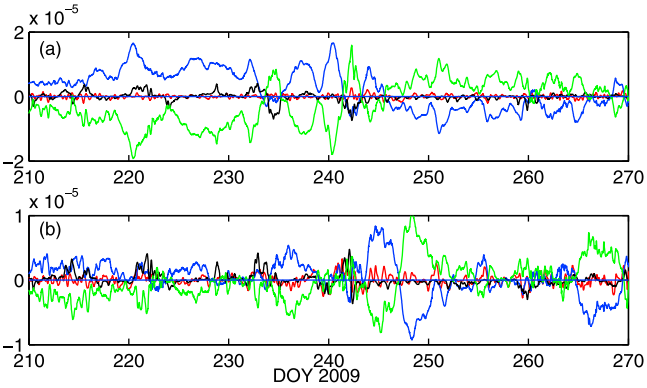

Figure 16. Depth-integrated momentum balance terms for (a) offshore and (b) alongshore flow, as estimated from the ADCP and Michigan City wind data (which were not available prior to DOY 210). Shown are the Coriolis parameter (blue), pressure gradient (green), wind stress (black), and acceleration (red), as defined in text.

the bottom stress is negligible, especially for the weak offshore flow. The free surface pressure gradients ($g\ \partial\eta/\partial x$, $g\ \partial\eta/\partial y$) are calculated as the residual of the balance; strictly speaking, these terms are the full pressure gradients and include a barotropic and baroclinic component, but an independent estimation of these gradients using the momentum balance of the surface mixed layer confirmed that the barotropic (free surface) component was dominant.

[48] Figure 16 shows the calculated terms for the depth-integrated alongshore and offshore momentum balances. The offshore flow is seen to be mostly in geostrophic balance during the period of strong alongshore flow, with offshore wind stress playing only a small role in the *local* balance (acceleration and bottom drag are negligible because of the weak offshore velocities). The circulation regime change discussed earlier is clearly manifested as a change in the cross-shelf pressure gradient at DOY 242. The strong alongshore flow during the time of persistent partial upwelling is also seen to be mostly in geostrophic balance, but the wind stress can at times play an important role in the local dynamics. The lower layer alongshore flow during this time can also be shown to be in geostrophic balance, but with the tilted thermocline reducing the cross-shelf pressure gradient such that flow in the lower layer is substantially weaker than the surface layer (Figure 15).

[49] To some extent, these features mimic the baroclinic coastal jet associated with a quasi-steady wind as described in detail by *Csanady* [1976] and *Csanady and Scott* [1974] for Lake Ontario and more generally by *Csanady* [1975] for coastal systems. As observed in the Great Lakes, the baroclinic coastal jet is a nearshore region of concentrated momentum that is part of a basin-wide response to strong alongshore winds (Kelvin waves become important for the full unsteady response). For the thermal observations here, the importance of this jet lies with the associated thermocline tilt.

4.5. Internal Kelvin Waves

[50] While internal Kelvin waves were hypothesized to be responsible for some of the nearshore thermal variability observed during the experiment, a linkage between propagating internal Kelvin waves and the observed thermal variability could not be established. A fairly comprehensive analysis that utilized many municipal water intake temperature time series around southern Lake Michigan (not presented) did not clearly show internal Kelvin wave propagation during the experiment. It was hypothesized that internal Kelvin waves would propagate from Illinois and Wisconsin into Indiana waters, but this could not be proved; the experimental design did not allow for the testing of this hypothesis, and water intake records proved to be too noisy to clearly correlate features from one intake to the next.

[51] Close inspection of SST satellite imagery identified a persistent, broad upwelling region along the Wisconsin coast during the experiment, but Kelvin waves were not observed to propagate to the study location. This does not preclude internal Kelvin waves from having propagated and caused some of the observed thermal variability in Indiana waters; it is entirely possible that subsurface internal Kelvin waves propagate, with no surface signature, along Lake Michigan and other Great Lakes coasts. Additionally, satellite imagery resolution precludes the detection of small-scale upwelling events caused by Kelvin waves. Additional experiments should be carried out to further investigate the existence of internal Kelvin waves and their influence on shores of various orientations.

5. Summary and Conclusions

[52] An experiment was carried out in southern Lake Michigan near Michigan City, Indiana (United States), to quantify the cross-shelf and temporal variability of nearshore temperatures during the stratified period, and to identify the causes of this variability. The experiment was successful in quantifying the nearshore thermal variability at this location, and characterizing many of the fundamental physical processes that occurred during the experiment that led to the observed variability.

[53] Thermocline motions were seen to create a broad lateral zone of thermal variability across the lake shelf. The level of variability seen at a particular location across the lake shelf was set by the relative proximity of the thermocline; for the southern lakeshore of Lake Michigan, the thermocline was seen to be roughly located 3–7 km offshore (when defined by the 12°C and 18°C isotherms). However, for much of the experiment the thermocline was partially upwelled, moving the zone of thermal variability to shallow waters within 2 km of shore. It was shown that the width of the observed zone of elevated thermal variability scaled roughly as the thickness of the thermocline projected onto the (relatively mild) lake bed slope, which may allow for estimates of thermal variability at other locations.

[54] Near-bottom thermal variability decreased monotonically with distance from shore during the strongly stratified period; as stratification weakened, both the thermal variability and its cross-shelf variability also decreased. As quantified using continuous temperature fluctuation statistics, the mooring closest to shore saw 24 h temperature changes in excess of 15°C, and 3 h changes in excess of 10 C, which is partially a consequence of the strong stratification observed at this site ($N \sim 10^{-2}\ \mathrm{s}^{-1}$). This variability has presumed importance for setting benthic species

distributions along the lake shelf, and it is of interest to quantify this variability along other Great Lakes coasts.

[55] Near-inertial internal Poincaré waves were present throughout the experiment, with modest thermocline displacements of several meters, and events lasting less than a week (a detailed account of these waves will be presented elsewhere). An ADCP located in the inertial boundary layer showed pervasive, often dominant, near-inertial clockwise motions, and analysis of the vertical structure of the currents indicated that these waves were predominantly vertical mode 1. During periods of elevated Poincaré wave activity, the thermocline was seen to migrate up and down the lake shelf over distances exceeding 2 km. These observations provide new insight into the properties of these waves near boundaries, which are not well understood.

[56] Although the study site is not aligned to be upwelling-favorable relative to the dominant southerly summer winds, several full upwellings were observed. These events were modest in both their offshore extent (generally less than 2.5 km) and duration (generally less than 2 days). Importantly, these upwellings were correlated with the few alongshore wind events that did occur, and a simple scaling of the Ekman transport-induced displacement of the coastal front agreed well with the observed front positions.

[57] For much of the strongly stratified period, the flow was seen to be alongshore and strong, and associated with a persistently upwelled orientation of the thermocline. This feature was barotropic in nature, and an estimation of the depth-integrated momentum balance during this period indicated that it was maintained by an alongshore pressure gradient and not the wind. Cross-shelf flow was a strong geostrophic balance between the cross-shelf free surface pressure gradient and the Coriolis force from the swift alongshore flow, with reduced flow below the thermocline on account of the upwelled thermocline and the opposing cross-shelf baroclinic pressure gradient it provided. A strong current reversal abruptly ended this feature. What is not known is the relationship between this feature (coastal jet and associated upwelled thermocline) and the larger, basin-scale circulation patterns, since the role of basin-wide winds on local circulation at this site is quite indirect.

[58] It was hypothesized that internal Kelvin waves would be largely responsible for observed thermal variability at the field site. Although tested, no evidence was found to support this hypothesis. However, additional work should be carried out to further investigate this hypothesis since the experimental configuration was not optimized for Kelvin wave detection. A comprehensive analysis of municipal water intake data and satellite sea surface temperature fields did not show Kelvin waves propagating from Wisconsin or Illinois to the Indiana shore. These data did reveal a broad, persistent upwelling zone along the Wisconsin coast for much of the experiment, consistent with earlier studies on upwelling in Lake Michigan [*Plattner et al.*, 2006]. Possible reasons for the lack of Kelvin wave propagation from Wisconsin to Illinois/Indiana might include the irregular southern Lake Michigan bathymetry and abrupt coastline curvature, but at this point all that can be definitively concluded is that SST imagery and water intake data did not show any Kelvin wave propagation along the southern Lake Michigan coastline.

[59] **Acknowledgments.** The authors wish to thank the crew of the NOAA GLERL R/V *Laurentian* for their help with mooring deployment and recovery. Tsung-Chan Hsieh, John Newton, and Mallory Barkdull provided helpful assistance with instrument programming and servicing. This work was supported by the Lake Michigan Coastal Program of the Indiana Department of Natural Resources and by the Physical Oceanography Division of the National Science Foundation, grant OCE-1030842. This is GLERL contribution 1615.

References

Antenucci, J. P., and J. Imberger (2001), Energetics of long internal gravity waves in large lakes, *Limnol. Oceanogr.*, *46*(7), 1760–1773, doi:10.4319/lo.2001.46.7.1760.

Antenucci, J. P., J. Imberger, and A. Saggio (2000), Seasonal evolution of the basin-scale internal wave field in a large stratified lake, *Limnol. Oceanogr.*, *45*(7), 1621–1638, doi:10.4319/lo.2000.45.7.1621.

Austin, J. A., and S. J. Lentz (2002), The inner shelf response to wind-driven upwelling and downwelling, *J. Phys. Oceanogr.*, *32*, 2171–2193, doi:10.1175/1520-0485(2002)032<2171:TISRTW>2.0.CO;2.

Beletsky, D., and D. J. Schwab (2001), Modeling circulation and thermal structure in Lake Michigan: Annual cycle and interannual variability, *J. Geophys. Res.*, *106*(C9), 19,745–19,771, doi:10.1029/2000JC000691.

Beletsky, D., and D. J. Schwab (2008), Climatological circulation in Lake Michigan, *Geophys. Res. Lett.*, *35*, L21604, doi:10.1029/2008GL035773.

Beletsky, D., W. P. O'Connor, D. J. Schwab, and D. E. Dietrich (1997), Numerical simulation of internal Kelvin waves and coastal upwelling fronts, *J. Phys. Oceanogr.*, *27*, 1197–1215, doi:10.1175/1520-0485(1997)027<1197:NSOIKW>2.0.CO;2.

Beletsky, D., D. J. Schwab, and M. J. McCormick (2006), Modeling the 1998–2003 summer circulation and thermal structure in Lake Michigan, *J. Geophys. Res.*, *111*, C10010, doi:10.1029/2005JC003222.

Csanady, G. T. (1972), Response of large stratified lakes to wind, *J. Phys. Oceanogr.*, *2*, 3–13, doi:10.1175/1520-0485(1972)002<0003:ROLSLT>2.0.CO;2.

Csanady, G. T. (1975), Hydrodynamics of large lakes, *Annu. Rev. Fluid Mech.*, *7*, 357–386, doi:10.1146/annurev.fl.07.010175.002041.

Csanady, G. T. (1976), Topographic waves in Lake Ontario, *J. Phys. Oceanogr.*, *6*, 93–103, doi:10.1175/1520-0485(1976)006<0093:TWILO>2.0.CO;2.

Csanady, G. T. (1977), Intermittent "full" upwelling in Lake Ontario, *J. Geophys. Res.*, *82*, 397–419, doi:10.1029/JC082i003p00397.

Csanady, G. T., and J. T. Scott (1974), Baroclinic coastal jets in Lake Ontario during IFYGL, *J. Phys. Oceanogr.*, *4*, 524–541, doi:10.1175/1520-0485(1974)004<0524:BCJILO>2.0.CO;2.

Donaldson, M. R., S. J. Cooke, D. A. Patterson, and J. S. Macdonald (2008), Cold shock and fish, *J. Fish Biol.*, *73*, 1491–1530, doi:10.1111/j.1095-8649.2008.02061.x.

Edwards, C. R., and H. E. Seim (2008), Complex EOF analysis as a method to separate barotropic and baroclinic velocity structure in shallow water, *J. Atmos. Oceanic Technol.*, *25*, 808–821, doi:10.1175/2007JTECHO562.1.

Gill, A. E. (1982), *Atmosphere-Ocean Dynamics*, Academic, London.

Gómez-Giraldo, A., J. Imberger, and J. P. Antenucci (2006), Spatial structure of the dominant basin-scale internal waves in Lake Kinneret, *Limnol. Oceanogr.*, *51*(1), 229–246, doi:10.4319/lo.2006.51.1.0229.

Haffner, G. D., M. L. Yallop, D. N. Hebert, and M. Griffiths (1984), Ecological significance of upwelling events in Lake Ontario, *J. Great Lakes Res.*, *10*, 28–37, doi:10.1016/S0380-1330(84)71804-1.

Hawley, N. (2004), Response of the benthic nepheloid layer to near-inertial internal waves in southern Lake Michigan, *J. Geophys. Res.*, *109*, C04007, doi:10.1029/2003JC002128.

Heufelder, G. R., D. J. Jude, and F. J. Tesar (1982), Effects of upwelling on local abundance and distribution of larval alewife (*Alosa pseudoharengus*) in eastern Lake Michigan, *Can. J. Fish. Aquat. Sci.*, *39*, 1531–1537, doi:10.1139/f82-205.

Lee, C. H., and N. Hawley (1998), The response of suspended particulate material to upwelling and downwelling events in southern Lake Michigan, *J. Sediment. Res.*, *68*, 819–831.

Liu, P. C., and G. S. Miller (1996), Wavelet transforms and ocean current data analysis, *J. Atmos. Oceanic Technol.*, *13*, 1090–1099, doi:10.1175/1520-0426(1996)013<1090:WTAOCD>2.0.CO;2.

Mortimer, C. H. (2004), *Lake Michigan in Motion-Responses of an Inland Sea to Weather, Earth-Spin, and Human Activities*, Univ. of Wis. Press, Madison.

Mortimer, C. H. (2006), Inertial oscillations and related internal beat pulsations and surges in Lakes Michigan and Ontario, *Limnol. Oceanogr.*, *51*(5), 1941–1955, doi:10.4319/lo.2006.51.5.1941.

Murthy, C. R., and D. S. Dunbar (1981), Structure of the flow within the coastal boundary layer of the Great Lakes, *J. Phys. Oceanogr.*, *11*, 1567–1577, doi:10.1175/1520-0485(1981)011<1567:SOTFWT>2.0.CO;2.

Plattner, S., D. M. Mason, G. A. Leshkevich, D. J. Schwab, and E. S. Rutherford (2006), Classifying and forecasting coastal upwellings in Lake Michigan using satellite derived temperature images and buoy data, *J. Great Lakes Res.*, *32*, 63–76, doi:10.3394/0380-1330(2006)32[63:CAFCUI]2.0.CO;2.

Rao, Y. R., and R. C. Murthy (2001a), Coastal boundary layer characteristics during summer stratification in Lake Ontario, *J. Phys. Oceanogr.*, *31*, 1088–1104, doi:10.1175/1520-0485(2001)031<1088:CBLCDS>2.0.CO;2.

Rao, Y. R., and C. R. Murthy (2001b), Nearshore currents and turbulent exchange processes during upwelling and downwelling events in Lake Ontario, *J. Geophys. Res.*, *106*(C2), 2667–2678, doi:10.1029/2000JC900149.

Rao, Y. R., and C. R. Murthy (2001c), Comparative analysis of spectral, empirical orthogonal function, and wavelet decompositions for an upwelling front, *J. Atmos. Oceanic Technol.*, *18*, 704–710, doi:10.1175/1520-0426(2001)018<0704:CAOSEO>2.0.CO;2.

Rao, Y. R., and D. J. Schwab (2007), Transport and mixing between the coastal and offshore waters in the Great Lakes: A review, *J. Great Lakes Res.*, *33*, 202–218, doi:10.3394/0380-1330(2007)33[202:TAMBTC]2.0.CO;2.

Rueda, F. J., S. G. Schladow, and S. O. Pálmarsson (2003), Basin-scale internal wave dynamics during a winter cooling period in a large lake, *J. Geophys. Res.*, *108*(C3), 3097, doi:10.1029/2001JC000942.

Saylor, J. H., and G. S. Miller (1988), Observation of Ekman veering at the bottom of Lake Michigan, *J. Great Lakes Res.*, *14*, 94–100, doi:10.1016/S0380-1330(88)71536-1.

Saylor, J. H., J. C. K. Huang, and R. O. Reid (1980), Vortex modes in southern Lake Michigan, *J. Phys. Oceanogr.*, *10*, 1814–1823, doi:10.1175/1520-0485(1980)010<1814:VMISLM>2.0.CO;2.

Schwab, D. J. (1977), Internal free oscillations in Lake Ontario, *Limnol. Oceanogr.*, *22*(4), 700–708, doi:10.4319/lo.1977.22.4.0700.

Tilburg, C. E. (2003), Across-shelf transport on a continental shelf: Do across-shelf winds matter?, *J. Phys. Oceanogr.*, *33*, 2675–2688, doi:10.1175/1520-0485(2003)033<2675:ATOACS>2.0.CO;2.

Trowbridge, J. H., and S. J. Lentz (1998), Dynamics of the bottom boundary layer on the northern California shelf, *J. Phys. Oceanogr.*, *28*, 2075–2093, doi:10.1175/1520-0485(1998)028<2075:DOTBBL>2.0.CO;2.

Wells, M. G., and S. Parker (2010), The thermal variability of the waters of Fathom Five National Marine Park, Lake Huron, *J. Great Lakes Res.*, *36*, 570–576, doi:10.1016/j.jglr.2010.04.009.

Wilson, K. A., E. T. Howell, and D. A. Jackson (2006), Replacement of zebra mussels by quagga mussels in the Canadian nearshore of Lake Ontario: The importance of substrate, round goby abundance, and upwelling frequency, *J. Great Lakes Res.*, *32*, 11–28, doi:10.3394/0380-1330(2006)32[11:ROZMBQ]2.0.CO;2.

Wüest, A., and A. Lorke (2003), Small-scale hydrodynamics in lakes, *Annu. Rev. Fluid Mech.*, *35*, 373–412, doi:10.1146/annurev.fluid.35.101101.161220.

S. Ahmed and C. D. Troy, School of Civil Engineering, Purdue University, 550 Stadium Mall Dr., West Lafayette, IN 47907-2051, USA. (troy@purdue.edu)

A. Goodwell, Ven Te Chow Hydrosystems Laboratory, University of Illinois at Urbana-Champaign, 301 N. Matthews Ave., Urbana, IL 61801, USA.

N. Hawley, Great Lakes Environmental Research Laboratory, NOAA, 4840 S. State Rd., Ann Arbor, MI 48108, USA.